Materials Advances

ROYAL SOCIETY OF CHEMISTRY

PAPER

View Article Online
View Journal | View Issue

Cite this: *Mater. Adv.*, 2022, 3, 6529

Correlating doping with the stability and color rendition of red phosphors†

Shuqin Chang,[a] Jipeng Fu,*[ab] Kaina Wang,[b] Xuan Sun,[ab] Yingying Ma,[a] Guangcan Bai,[c] Guoquan Liu,[c] Yonggang Wang[a] and Mingxue Tang*[a]

Received 1st June 2022,
Accepted 4th July 2022

DOI: 10.1039/d2ma00617k

rsc.li/materials-advances

Although near-infrared phosphors have been widely reported, discovering efficient red-emitting phosphor materials with superior photophysical properties and high color quality is still a challenge for optimizing white light-emitting diodes (wLEDs). In this regard, a series of Eu^{2+} and Ce^{3+} doped SrS phosphors were synthesized *via* a one-step solid-state method at 1100 °C. The SrS:$(Eu^{2+})_n$ and SrS:$(Ce^{3+})_{0.01}$,$(Eu^{2+})_n$ powders show substantial spectral broadening (~80 nm) along with a significant thermal quenching resistance. The phosphor of SrS:$(Eu^{2+})_{0.002}$ exhibits the most intense luminescence with a high color purity of 99.94% and an afterglow luminescence lasting several seconds. The luminescence intensity and peak position were modulated by the resonance-type energy transfer from Ce^{3+} to Eu^{2+} ions, which is proposed to follow the dipole–dipole interaction mechanism by Dexter's energy transfer theory and Reisfeld's approximation. The outstanding photoluminescence properties of Eu^{2+} are attributed to the nephelauxetic effect and crystal field splitting of rock-salt. The wLED device of SrS:$(Eu^{2+})_{0.05}$ packaged with a blue chip and $(Sr,Ba)_2SiO_4$:Eu^{2+} shows a super-high color rendering index of 87.9, suggesting great potential for superior luminescence and promising wide applications.

1. Introduction

Commercial phosphor-converted white light-emitting diodes (pc-wLEDs) are composed of a blue InGaN LED chip and yellow YAG:Ce^{3+} phosphors and extensively used in many fields due to their low energy consumption, great durability and safety.[1–4] However, YAG:Ce^{3+} lacks photoluminescence in the red spectral range, leading to an inferior color rendering index (CRI) and correlated color temperature (CCT).[5–7] Numerous red-emitting phosphors have recently attracted extensive attention in achieving high-quality pc-wLEDs.

Due to their red bands and allowed d–f transition, the highly efficient Eu^{2+}-activated phosphors have been rapidly developed in the past years. The narrow-band red-emitting phosphor $SrLiAl_3N_4$:Eu^{2+} showed emission at λ_{max} ~ 650 nm with a full-width at half-maximum (FWHM) of ~1180 cm^{-1} (~50 nm), >95% relative quantum efficiency at 200 °C and a color rendition of $R_a8 = 91$.[3] Liu's group reported a more facile method to obtain $SrLiAl_3N_4$:Eu^{2+} under a mixed gas of 90% N_2 and 10% H_2, showing emission at λ_{max} ~650 nm with a FWHM of ~1279 cm^{-1} (55 nm) and a CRI of 91.1 ($R9 = 68$).[8] However, those phosphors exhibited a narrow emission band and exceeded infrared emission, making them less than optimal for high-quality lighting applications. Based on the crystallization of aluminosilicate glass, Hu *et al.* synthesized the red-emitting $Mg_2Al_4Si_5O_{18}$:Eu^{2+} bulk phosphor with a broad emission band (λ_{max} ~ 620 nm, FWHM ~ 100 nm), and CRI (R_a = 85.2).[1] However, the emission intensity of $Mg_2Al_4Si_5O_{18}$:Eu^{2+} decreases by almost 40% from 77 K to 502 K and the detailed insights into the relationship between the structural variation and luminescent properties need to be further investigated. Many researchers have focused on CaS:Eu^{2+} phosphors, which exhibit intense photo-stimulated luminescence at λ ~ 650 nm with a long-wavelength tail in the near-infrared region (600–800 nm). This feature may fail to meet the expectations in the field of pc-wLEDs. The substitution of Ca with Sr leads to a substantial blueshift and plays an important role in the discovery of broad band visible-light phosphors.[9–11]

Herein, Eu^{2+} and Ce^{3+} were successfully incorporated into SrS with sulfur as a source material for the first time *via* a facile one-step solid-state approach at 1100 °C.[12–15] Additionally, powder X-ray diffraction (PXRD) and continuous wave-electron paramagnetic resonance (CW-EPR) were carried out

[a] *Center for High Pressure Science and Technology Advanced Research, Beijing, 100094, China. E-mail: fujipeng@cjlu.edu.cn, mingxue.tang@hpstar.ac.cn*
[b] *Key Laboratory of Rare Earth Optoelectronic Materials and Devices of Zhejiang Province, Institute of Optoelectronic Materials and Devices, Hangzhou, 310018, China*
[c] *State Key Laboratory of Natural and Biomimetic Drugs, School of Pharmaceutical Sciences, Peking University, Beijing, 100191, China*

† Electronic supplementary information (ESI) available: The Supporting Information is available online or on request from the authors. Additional elemental ratio; table of FWHM, CIE and color purity; diffuse reflectance spectra and electroluminescence spectrum of the SrS:$(Eu^{2+})_{0.05}$ phosphor-based wLED are attached. See DOI: https://doi.org/10.1039/d2ma00617k

to probe the local coordination in the host material. The intensity of the luminescence for the target materials was ostensibly tailored by the introduction of Eu^{2+} and Ce^{3+}, which can be easily adjusted to optimize industrial mass production by way of energy transformation. Under $\lambda \sim 430$ nm light excitation, the designed SrS:$(Eu^{2+})_n$ and SrS:$(Ce^{3+})_{0.01}$,$(Eu^{2+})_n$ phosphors give a broad band emission peak in the orange-red region, which is favorable for pc-WLEDs. The as-fabricated pc-WLEDs with CCT = 2819 K, CRI = 82.6 and R_a = 87.9 present superior thermal stability, enabling their reliability and color rendition for white light source applications.

2. Experimental section

2.1 Materials and reagents

Strontium carbonate ($SrCO_3$, 99.5%), cerium oxide (CeO_2, 99.9%) and europium oxide (Eu_2O_3, 99.9%) were purchased from Macklin and sulfur flowers (S, 99.999%) were purchased from Aladdin. The commercial green phosphor $(Sr,Ba)_2SiO_4:Eu^{2+}$ and the chip (λ = 430 nm) were purchased from Shenzhen Looking Long Technology Co., Ltd. All the chemicals were used without further purification.

2.2 Synthesis of the SrS phosphor

A series of SrS:nEu^{2+} phosphors with different Eu^{2+} content (n = 0.005–0.05) were synthesized by employing a solid-state reaction method. The experimental steps were as follows: $SrCO_3$, Eu_2O_3 and S with a $1:n:2.5$ mole ratio were ground in a mortar for 30 minutes to obtain uniform mixtures. Then, the mixtures were loaded in a large alumina crucible with a thin layer of carbon powder and sintered at 1100 °C for 2 hours in a high-temperature box furnace under air atmosphere. Finally, the obtained samples were cooled to room temperature in the furnace and were reground for 5 minutes for further measurement. Other samples were based on the same method of preparation.

2.3 Characterization

The powder X-ray diffraction patterns of the phosphors to study their crystal structures were recorded using an XRD diffractometer (PANalytical Empyrean) operating with CuK_α radiation (λ = 1.5406 Å) at 40 kV and 40 mA. The morphologies of the powders were analyzed by field-emission scanning electron microscopy (FE-SEM; JSM-7900F) and the elemental mapping was performed using EDX attached to the FE-SEM. The photoluminescence emission (PL) and excitation (PLE) spectra at room temperature of all samples were recorded using a lifetime and steady-state spectrometer (FLS980, Edinburgh Instruments Ltd) equipped with a Xe lamp. The thermal quenching properties were evaluated by an EX-1000 spectrometer (EVERFINE, China). The reflectance spectra at room temperature of all samples were collected using a UV-3600plus (Shimadzu).

Continuous wave-electron paramagnetic resonance (CW-EPR) analysis was performed on a Bruker A200 spectrometer. The following parameters were used: sweep field range, 100 G; sweep time, 60 s; modulation amplitude, 1 G; modulation frequency, 100 kHz; and microwave power, 19.23 mW.

The wLED structures were fabricated using the commercial green phosphor $(Sr,Ba)_2SiO_4:Eu^{2+}$ and LED chips (λ = 430 nm). The phosphors were mixed with a commercial AB silicone glue (glue A:hardener B = 1 : 4, AB silicone glue:as-synthesized phosphors:green phosphors = 10 : 2 : 1.5). The obtained phosphor–glue mixture was coated on the LED chips and then cured at 100 °C for 1 h. The properties of the fabricated wLEDs were measured by a HAAS-2000 photoelectric measuring system (380–780 nm, EVERFINE, China). The forward bias current was 99.94 mA.

3. Results and discussion

The crystal structure and phase identification of SrS with various contents of Eu^{2+} (SrS:$(Eu^{2+})_n$, n = 0.005–0.05) were investigated by PXRD. As shown in Fig. 1a, all diffraction peaks are well indexed by a cubic cell ($Fm\bar{3}m$) and are consistent with those of the SrS rock-salt phase (PDF card No. 08-0489), demonstrating that the doping of Eu^{2+} (n = 0.005–0.05) into the SrS host lattice does not destroy the original crystal structure (Fig. 1b). The phenomenon can be explained using Bragg's law:

$$2d \sin\theta = n\lambda \quad (1)$$

In this equation, d, θ, n and λ are defined as the distance between successive atoms, diffraction angle, diffraction order and the wavelength, respectively. Furthermore, the maintenance of the structure is assumed by the calculations of the radius percentage difference (Dr) between the doped and substituted ions (eqn (2)), which must not exceed 30%:[16]

$$\mathrm{Dr} = 100 \times \frac{R_m(\mathrm{CN}) - R_d(\mathrm{CN})}{R_m(\mathrm{CN})} \quad (2)$$

where CN is the coordination number and R_m(CN) and R_d(CN) denote the radii of the matrix ion and doped ion, respectively. The calculated values of Dr are listed in Table 1, where the Dr between Eu^{2+} and Sr^{2+} is within 10%, much smaller than 30%. Thus, the Eu^{2+} dopant will prefer to substitute the Sr^{2+} sites. The scanning electron microscopy (SEM) images (Fig. 1) present average sizes of 10–30 μm for the SrS:$(Eu^{2+})_{0.002}$ particles with a smooth surface, which may facilitate the luminescent properties when incorporated into LED packages.[17] Elemental mapping and energy dispersive X-ray spectroscopy (EDS) were also conducted and their images are shown in Fig. 1 and Fig. S1, (ESI†) respectively. Obviously, all the Sr, S and Eu elements were homogeneously distributed. The atomic percentages of Sr and S are roughly determined to be 52% and 48%, respectively, consistent with the expected values from the solid-state preparation.

Fig. 2 presents the luminescent properties of SrS:$(Eu^{2+})_n$ at room temperature. The materials can be excited by ultraviolet (UV) and green lights. Under excitation at $\lambda \sim 430$ nm (Fig. 2a), the concentration-dependent photoluminescence emission (PL) spectra of SrS:$(Eu^{2+})_n$ show the characteristic broad band in the range of 570–730 nm with the main signal around

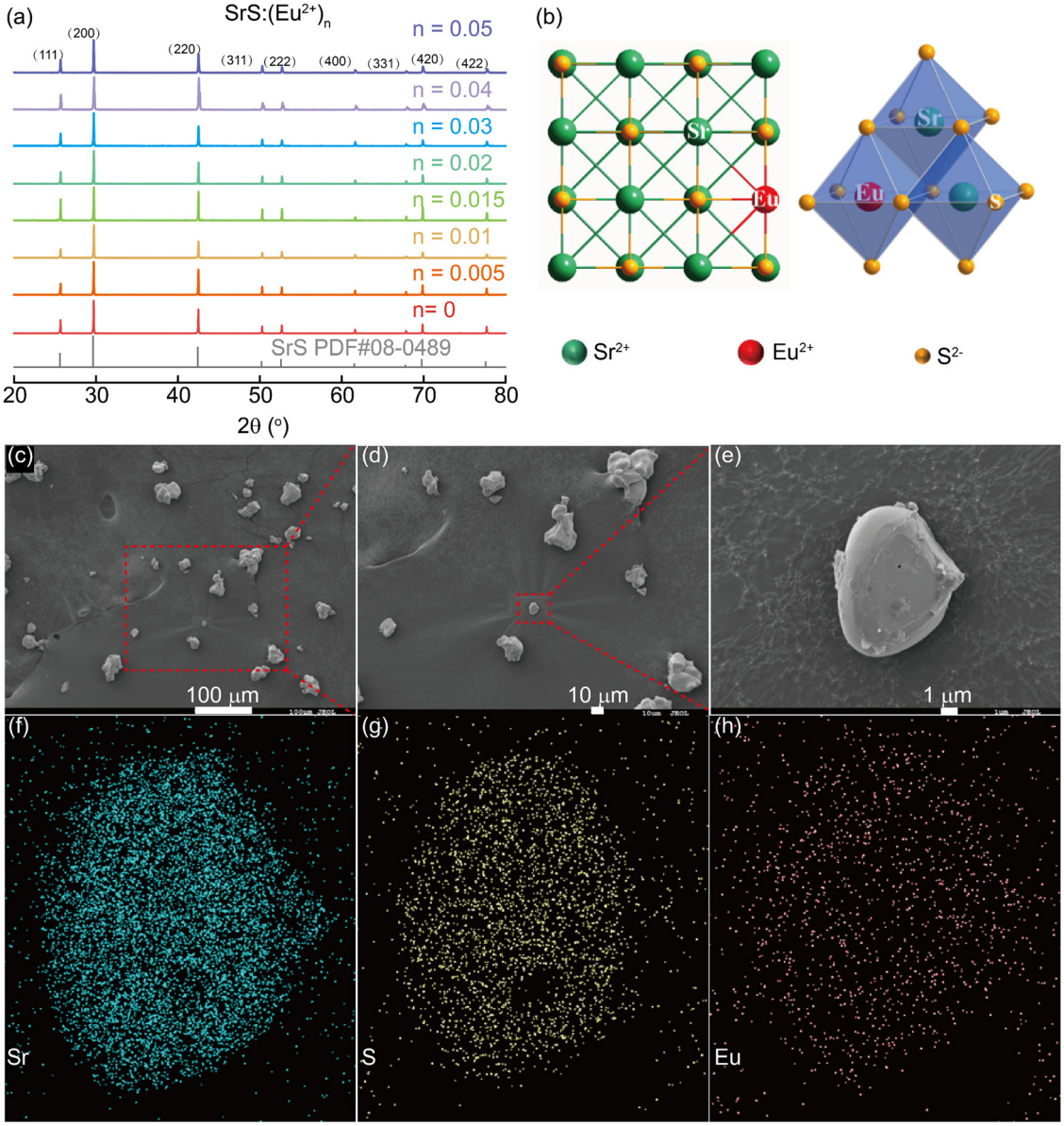

Fig. 1 (a) X-ray diffractograms of SrS with various contents of Eu^{2+}. (b) A crystal structure model of SrS:$(Eu^{2+})_n$. (c and d) SEM images of SrS with 0.2 mol% Eu^{2+} dopant and (e) an enlarged particle. (f–h) Elemental mapping images of Sr, S and Eu in the selected particle.

Table 1 Ionic radii difference percentage between the matrix and doped ions

		Difference % between ionic radii		
Dopant	Radii/Å (CN)	Sr^{2+} 1.18(6)	Sr^{2+} 1.26(8)	Sr^{2+} 1.31(9)
Eu^{2+}	1.17(6)	0.8	7.1	10.7
Eu^{2+}	1.25(8)	−5.9	0.8	4.6
Eu^{2+}	1.30(9)	−10.2	−3.2	0.8

620 nm. This signal is attributed to the radiative de-excitation of the lowest excited state $4f^65d^1$ electronic configuration to the $^8S_{7/2}$ ground state $4f^7$ of Eu^{2+} ($4f^65d^1 \rightarrow 4f^7$).[18,19] Because the 5d energy levels of Eu^{2+} are sensitive to the bond lengths, coordination numbers and symmetry of the host, it is feasible to prepare a phosphor with a specific emission color by many strategies such as cation-size-mismatch and cation substitution.[2,20–22] The broad band is due to the strong crystal field by the distorted coordination environments of the Eu^{2+} emission centers.[23] The emission band is further deconvoluted into only one Gaussian profile, suggesting the presence of a single Eu^{2+} center.[24] As shown in Fig. 2b, the PL intensity grows at the beginning with increase in the concentration of Eu^{2+}, and it reaches a maximum when the concentration is equal to 0.002 (molar ratio). The intensity decreases with further increasing Eu^{2+} concentration. However, the PL spectra exhibit a consecutive redshift from orange-red to red, with the peak shifting from $\lambda \sim 615$ nm ($n = 0.0005$) to $\lambda \sim 628$ nm ($n = 0.05$). The peak position tendency is related to the distance of the radius of Eu^{2+}, which can

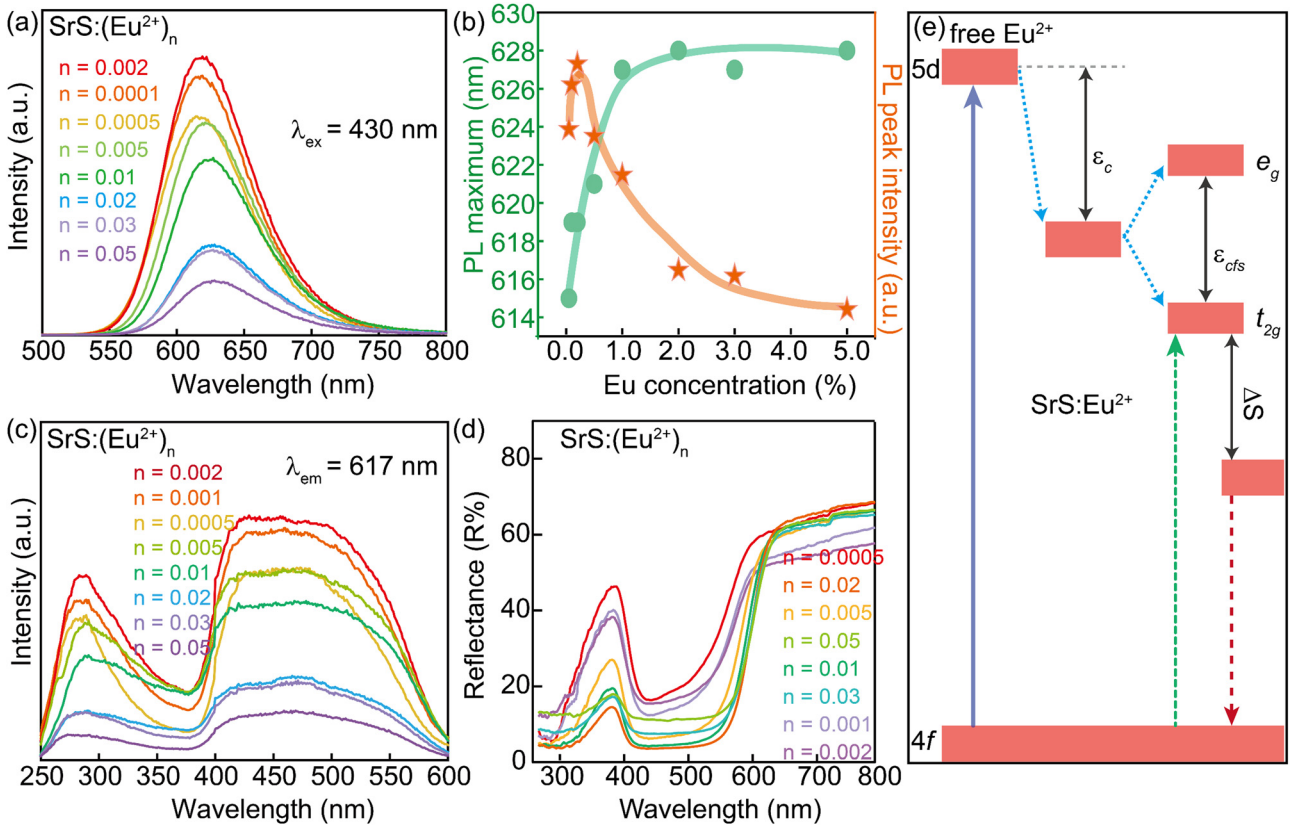

Fig. 2 (a) PL spectra of SrS:$(Eu^{2+})_n$ under $\lambda \sim 430$ nm excitation. (b) Dependence of PL maximum position and PL peak intensity on Eu^{2+} concentration in SrS:$(Eu^{2+})_n$. The curves in (b) are guided by eye. (c) PLE spectra of SrS:$(Eu^{2+})_n$ under $\lambda \sim 617$ nm emission. (d) Diffuse reflectance spectra of SrS:$(Eu^{2+})_n$. (e) Schematic diagram for the degeneration of the free Eu^{2+} energy states in SrS: Eu^{2+} phosphors. The effects include the nephelauxetic effect (ε_c, centroid shift), crystal field splitting (ε_{cfs}) by the Jahn–Teller effect and Stokes shift (ΔS).

be quantified by Van Uitert's empirical eqn (3):[2,25]

$$E(\mathrm{cm}^{-1}) = Q * \left[1 - \left(\frac{V}{4}\right)^{1/V} \times 10^{-(nE_a r)/80}\right] \quad (3)$$

where E denotes the energy of the Eu^{2+} emission peak, Q^* is a constant and represents the energy position for the lower d-band edge of free Eu^{2+} ($Q^* = 34\,000$ cm^{-1}), V is the valency of Eu^{2+} ($V = 2$), n stands for the coordination number of Eu^{2+}, E_a is a constant and represents the electron affinity of the anion atoms, and r is the radius of the host cation that can be occupied by Eu^{2+}. Then, in the SrS:$(Eu^{2+})_n$ samples, E is proportional to r. Based on the above-mentioned points, the redshift phenomenon is attributed to the structural variation resulting from the substitution of Sr^{2+} ions by the Eu^{2+} ions with smaller radii.

The phosphor of SrS:$(Eu^{2+})_{0.002}$ can provide an absolute quantum yield (QY) of 36.05% and its FWHM is 76.5 nm (Table S1, ESI†). According to G. Blasse's function (eqn (4)), the critical distance of energy transfer (R_c) is calculated to be 37.32 Å.

$$R_c = 2\left(\frac{3V}{4\pi x_c N}\right)^{\frac{1}{3}} \quad (4)$$

where V is the volume of the unit cell, N is the number of total Eu^{2+} sites per unit cell and x_c is the critical concentration of the activator ion. In SrS, $V = 217.73$ Å^3, $N = 4$, and the critical concentration, x_c, is about 0.002 in our system. As the value of R_c is over 5 Å, the exchange interaction has no perceptible effect for non-radiative energy transfer processes between adjacent Eu^{2+} ions in the matrix. Thus, the concentration quenching mechanism in Eu^{2+}-doped SrS phosphors may have occurred due to dipole–dipole interactions.

Clearly, monitoring at $\lambda \sim 617$ nm, the photoluminescence excitation (PLE) spectra of SrS:$(Eu^{2+})_n$ afford an ultra-broad band in the range of $\lambda \sim 250$–600 nm (Fig. 2c). The main PLE spectra in the range of 400–600 nm indicate numerous transitions to the $4f^6 5d t_{2g}^1$ manifold of Eu^{2+} (Fig. 2e).[18,26] The weak band ($\lambda \sim 280$ nm) is attributed to the effective band–band transition in the SrS lattice.[27] No trace of Eu^{3+} emission is found for intervalence charge transfer (IVCT), which could quench the Eu^{3+} emission pairs with Eu^{2+} ions.[28] Fig. 2d displays the diffuse reflectance spectra of SrS:$(Eu^{2+})_n$, which show a broad absorption band (400–600 nm) in accordance with the PLE spectra mentioned before. A schematic diagram for the degeneration of the free Eu^{2+} energy states in the SrS:Eu^{2+} phosphors is shown in Fig. 2e. The 5d orbitals of Eu^{2+} split into two kinds of orbitals, e_g and t_{2g}, by the nephelauxetic effect and Jahn–Teller effect. The e_g states have higher energy than the t_{2g} states and the electron transition between the 4f state and the t_{2g} state shows a blue excitation band and red emission band with Stokes shift.

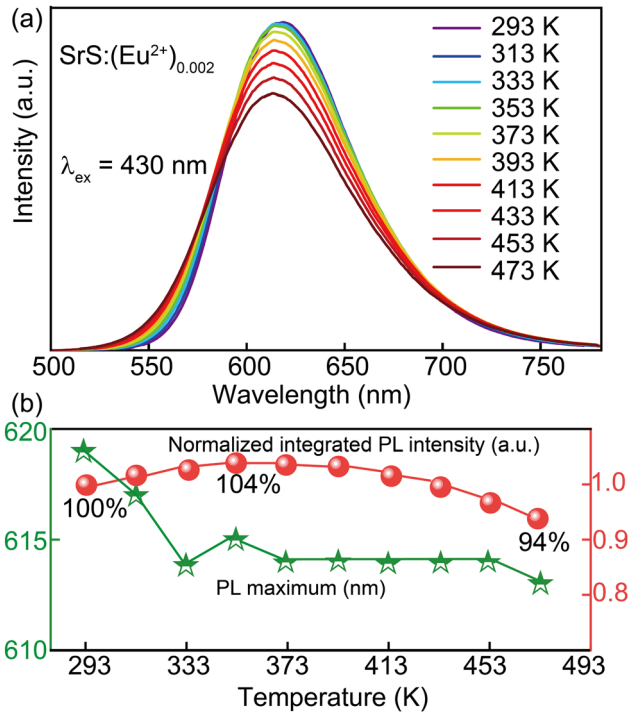

Fig. 3 Thermal stabilities of the SrS:$(Eu^{2+})_{0.002}$ phosphor. (a) PL spectra of SrS:$(Eu^{2+})_{0.002}$ under $\lambda \sim 430$ nm excitation in the temperature range of 293–473 K. (b) Normalized PL signal and PL maximum as a function of temperature; data from (a).

The thermal stability of the phosphors is crucial for pc-LED application and Fig. 3 demonstrates the thermal behavior of SrS:$(Eu^{2+})_{0.002}$ in the temperature range of 293 to 473 K. It shows that the normalized integrated PL intensity first increases and then decreases slowly with the increase in temperature due to the enhanced nonradiative transition probabilities. The normalized signal slowly rises to ~104% at 353 K to reach its maximum and then decreases to ~94% under further increasing temperature to 473 K. The PL maximum shows an obvious blueshift from 293 K ($\lambda \sim 619$ nm) to 333 K ($\lambda \sim 613$ nm) and then retains the same upon further increase in temperature. According to the Arrhenius equation (eqn (5)),[29] ΔE is found to be 0.18 eV at 293–373 K and 3.13 eV at 373–473 K by fitting the measured data. To the best of the knowledge, the higher the value of ΔE, the less energy is lost and more photons are utilized by the activator ions. This further validates the feasibility of creating high-power pc-LEDs with good thermal stability using SrS:$(Eu^{2+})_n$ phosphors.

$$I_T/I_0 = [1 + A \times \exp(-\Delta E/kT)]^{-1} \quad (5)$$

where I_T and I_0 represent the luminescent intensities at a chosen temperature and 293 K, respectively, ΔE is the activation energy, k is the Boltzmann constant (1.380649×10^{-23} J K^{-1}) and A is a constant.

Various approaches have claimed to tune the color of phosphors such as altering the doped ions, controlling the energy transfer (ET) process, and changing the matrix crystal field environment.[30–32] Among them, energy transfer between the co-doped activators is regarded as an effective strategy to achieve color-tunable emission. The energy donor (the sensitizer) accepts the incoming photon and emits it further, which can be again absorbed by the energy acceptor (the activator) to be re-emitted in the visible region.[33] The Ce^{3+} ion is an appropriate sensitizer for Eu^{2+} ions by transferring the excitation energy to the co-activators.[34] To check the influence of the co-activator, 0.01 Ce^{3+} was introduced into the phosphors of SrS:$(Ce^{3+})_{0.01}$,$(Eu^{2+})_n$ (n = 0.0001, 0.0005, 0.001, 0.005, 0.01 and 0.1). From the PXRD patterns (Fig. 4a), all major diffraction peaks of the Ce^{3+} and Eu^{2+} co-doped SrS match well with the pristine SrS rock-salt-like structure. According to Bragg's law (eqn (1)), the structural change caused by Ce^{3+} and Eu^{2+} co-doping is insignificant. The SEM morphological images and the elemental distribution are given in Fig. 4, in which the distribution of the different elements is uniform.

EPR is sensitive to probing the local electron configuration. As expected, in Fig. 4b, Eu^{2+} ($^8S_{7/2}$ ground state) in SrS:$(Eu^{2+})_{0.01}$ shows an isotropic EPR signal at g = 1.99, reflecting its coordination in the symmetric environment within the cubic crystalline. The serration located between the two peaks is attributed to the different hyperfine splitting caused by the magnetically non-equivalent pairs of ^{151}Eu and ^{153}Eu.[35–37] Further introduction of Ce^{3+} into SrS:$(Eu^{2+})_{0.01}$ enhanced the EPR signal, possibly due to the ET effect for promoting polarization between the different states of electron spin.

Fig. 5a depicts the PLE spectrum of SrS:$(Eu^{2+})_{0.001}$ and the PL spectrum of SrS:$(Ce^{3+})_{0.01}$. Clearly, there is a virtually ideal overlap ($\lambda \sim$ 460–600 nm) between the emission of Ce^{3+} and excitation of Eu^{2+}, where the resonance-type ET might occur from Ce^{3+} to Eu^{2+}. The ET evidence from Ce^{3+} to Eu^{2+} is plotted in Fig. 5b: the PL intensity of the co-doped particles (SrS:$(Ce^{3+})_{0.01}$,$(Eu^{2+})_{0.001}$) is obviously higher than that of the single-doped particles (SrS:$(Eu^{2+})_{0.001}$). Fig. 5c and d show the room-temperature PL and PLE spectra of SrS:$(Ce^{3+})_{0.01}$,$(Eu^{2+})_n$, respectively. Under the excitation of $\lambda \sim 430$ nm, the typical emission intensity of Eu^{2+} centered at $\lambda \sim 620$ nm is enhanced significantly, and it reaches a maximum intensity at n = 0.001 (Fig. S3, ESI†). Meanwhile, the characteristic emission intensity of Ce^{3+} located at $\lambda \sim 485$ nm decreases monotonously with increasing Eu^{2+} doping concentration. The emission peak wavelength exhibits a noticeable redshift from $\lambda \sim 612$ nm (n = 0.0001) to $\lambda \sim 629$ nm (n = 0.1) on adding more Eu^{2+} ions (Fig. S3, ESI†). From the measured PLE spectra monitored at $\lambda \sim 617$ nm, the co-doped phosphors have an optimal content of n = 0.001 Eu^{2+}. A schematic ET process diagram of Ce^{3+} and Eu^{2+} is shown in Fig. 5e. All the results prove that ET is expected in the phosphors of SrS:$(Ce^{3+})_{0.01}$,$(Eu^{2+})_n$ to enhance the red emission (Fig. 5f), which are suitable features for white LEDs excited by blue and UV light. The ET efficiency (η_T) from Ce^{3+} to Eu^{2+} can be computed by eqn (6).[38] The values of η_T are 0.84 and 0.88 in the SrS:$(Ce^{3+})_{0.01}$,$(Eu^{2+})_{0.005}$ and SrS:$(Ce^{3+})_{0.01}$,$(Eu^{2+})_{0.001}$ phosphors, respectively.

$$\eta_T = 1 - \frac{I_{s0}}{I_s} \quad (6)$$

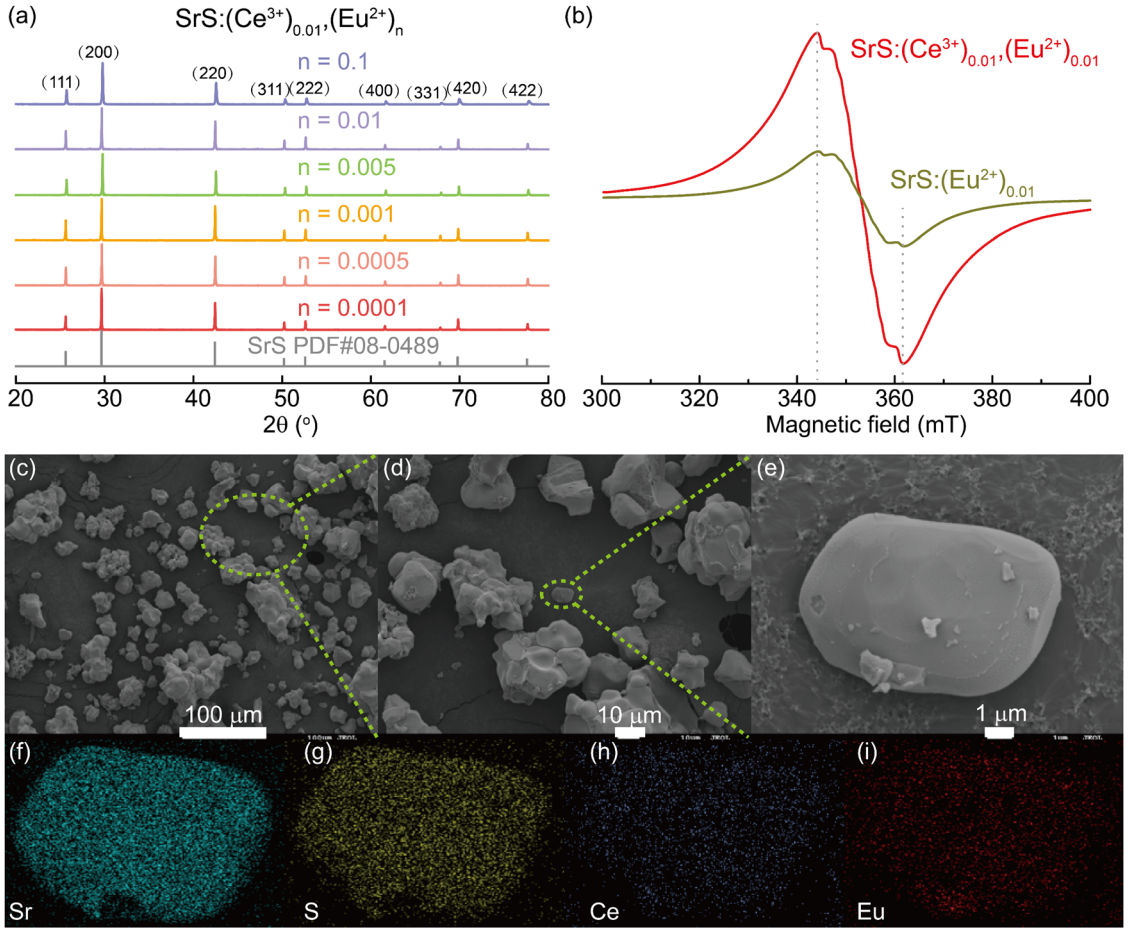

Fig. 4 (a) X-ray diffractograms of SrS:$(Ce^{3+})_{0.01}$ with different doping contents of Eu^{2+}. (b) Room-temperature CW-EPR of Eu^{2+} and Ce^{3+} doped SrS. (c and d) SEM images of SrS:$(Ce^{3+})_{0.01}$,$(Eu^{2+})_{0.001}$ and (e) an enlarged particle. (f–i) Elemental mapping images of Sr, S, Ce and Eu in the selected particle.

where I_{s0} and I_s present the luminescent intensity of Ce^{3+} without and with Eu^{2+} in the sample, respectively. The values of η_T are a function of Eu^{2+} content. Based on Dexter's energy transfer theory and Reisfeld's approximation, we can obtain the following proportional relationship:[39]

$$\frac{I_{s0}}{I_s} \propto C^{m/3} \quad (7)$$

where C is the content of Eu^{2+} and m depends on the type of interactions (m = 6 and 8 correspond to dipole–dipole and dipole–quadrupole interactions, respectively). We conclude that m = 6 is evidently correct and the ET from Ce^{3+} to Eu^{2+} follows the dipole–dipole mechanism.[33,40] The energy transfer mechanism *via* dipole–dipole interaction in SrS:Ce^{3+},Eu^{2+} is the same as that in CaS:Ce^{3+},Eu^{2+}.[41,42]

As mentioned above, the single Eu^{2+}-doped phosphors SrS:$(Eu^{2+})_n$ show broad band absorption, which leads to a red body color under natural light (Fig. 6a) and favors its application for blue light-pumped LEDs. Notably, a long afterglow is observed by the naked eye and lasts for several seconds (Fig. 6a). The materials SrS:$(Eu^{2+})_n$ turn brilliant red under natural light with the increase in Eu^{2+} dopant. Fig. 6a vividly depicts the Commission International de l'Eclairage (CIE) chromaticity coordinates of SrS:$(Eu^{2+})_n$ under $\lambda \sim 430$ nm excitation. These values are regularly shifted from orange-red (0.6271, 0.3723) to red (0.6589, 0.3408) as the concentration of Eu^{2+} varies from 0.0005 to 0.05. The CCT and high color purity (calculated by eqn (8)) of these samples are listed in Table S1 (ESI†). The CIE coordinates, CCT and color purity of the phosphors co-doped with Ce^{3+} and Eu^{2+} are also determined and portrayed in Fig. 6b and summarized in Table S2 (ESI†). It shows that the (x, y) of the samples changes from (0.5045, 0.4022) to (0.6559, 0.3426) and the color tone varies from orange to red. Compared with the Eu^{2+} single-doped samples, the CIE chromaticity coordinates of the SrS:$(Ce^{3+})_{0.01}$,$(Eu^{2+})_n$ phosphors shift to orange. Therefore, phosphors with excellent photoluminescence can be easily achieved by adjusting the concentration of the activators. We randomly selected the sample SrS:$(Eu^{2+})_{0.05}$ with lower PL intensity and combined the commercial green phosphor $(Sr,Ba)_2SiO_4$:Eu^{2+} and a blue InGaN LED chip (~430 nm) to fabricate wLEDs. The electroluminescence spectrum is illustrated in Fig. S5 (ESI†) and the device exhibits a warm white emission with excellent R_a = 87.9, CRI = 82.6 and low CCT = 2819 K. The results indicate that the phosphors exhibit controllable color tuning or hue for various potential applications and are highly promising candidates in

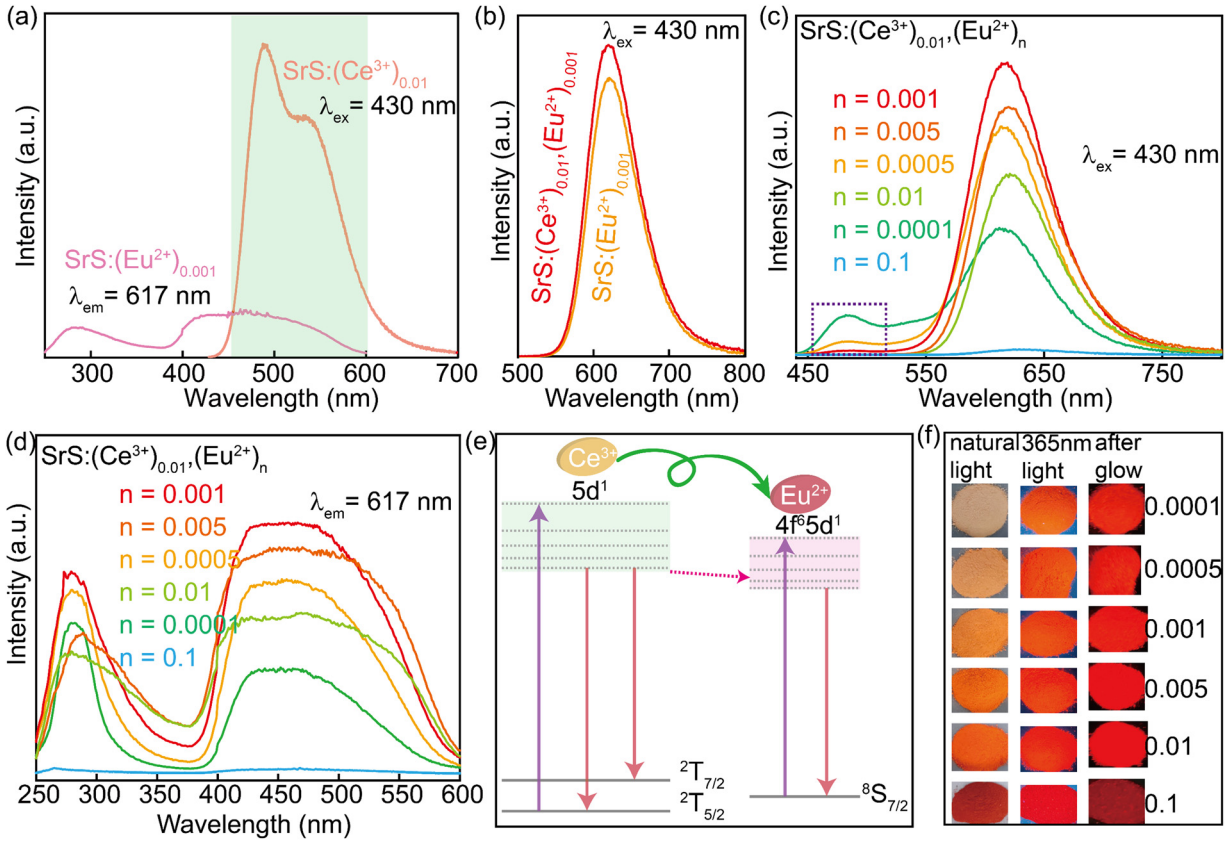

Fig. 5 (a) PL spectrum of SrS:$(Ce^{3+})_{0.01}$ under $\lambda \sim 430$ nm excitation and PLE spectrum of SrS:$(Eu^{2+})_{0.001}$ under $\lambda \sim 617$ nm emission. (b) PL spectra of SrS:$(Ce^{3+})_{0.01}$,$(Eu^{2+})_{0.001}$ and SrS:$(Eu^{2+})_{0.001}$ under $\lambda \sim 430$ nm excitation. (c) PL spectra of SrS:$(Ce^{3+})_{0.01}$,$(Eu^{2+})_n$ under $\lambda \sim 430$ nm excitation. (d) PLE spectra of SrS:$(Ce^{3+})_{0.01}$,$(Eu^{2+})_n$ under $\lambda \sim 617$ nm emission. (e) Schematic diagram showing the energy transfer process of SrS:$(Ce^{3+})_{0.01}$,$(Eu^{2+})_n$. (f) Optical images of SrS:$(Ce^{3+})_{0.01}$,$(Eu^{2+})_n$ phosphors under natural light, 365 nm light lamp and afterglow luminescence.

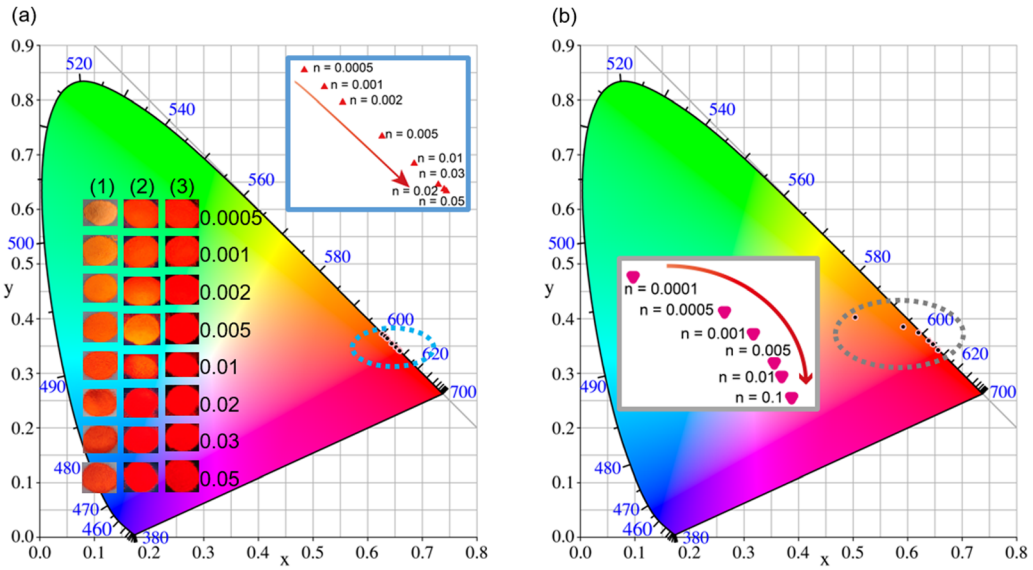

Fig. 6 (a) CIE chromaticity diagram of SrS:$(Eu^{2+})_n$. The inset shows optical images: (1), (2) and (3) denote the phosphors under natural light, 365 nm light and afterglow luminescence, respectively. (b) CIE chromaticity diagram of SrS:$(Ce^{3+})_{0.01}$,$(Eu^{2+})_n$. The inset shows the color trends with different Eu^{2+} content.

the illumination field.

$$\text{Color purity} = \frac{\sqrt{(x-x_i)^2+(y-y_i)^2}}{\sqrt{(x_d-x_i)^2+(y_d-y_i)^2}} \quad (8)$$

4. Conclusions

In summary, we have successfully designed and investigated the Eu^{2+}/Ce^{3+}-activated broad band red-emitting phosphors with $\lambda_{max} \sim 620$ nm based on the SrS host. The chemical structure of the phosphors is found to be highly stable and the introduction of Eu^{2+} and Ce^{3+} has a negligible effect on the crystal structure of the matrix. Taken together, the SrS:Eu^{2+} phosphors show broad band emission, superior color purity and great thermal stability up to 473 K. The doping of Ce^{3+} in SrS:Eu^{2+} effectively optimizes the luminescence properties *via* the dipole–dipole energy transfer mechanism. By combining the phosphor SrS:$(Eu^{2+})_{0.05}$ with the commercial green phosphor $(Sr,Ba)_2SiO_4$:Eu^{2+} and a blue InGaN LED chip, a warm wLED with an Ra of 87.9 and CRI of 82.6 is achieved. The experimental results show that SrS:Eu^{2+} and SrS:Ce^{3+},Eu^{2+} phosphors are promising candidates for the red component of wLEDs. Our work provides a general and facile synthetic strategy towards novel color-tunable bulk compounds and broadens the applications of rare earth sulfide phosphors.

Author contributions

S. Chang, K. Wang and X. Sun performed the material synthesis and structural characterizations; Y. Ma and Y. Wang contributed to the structural property analysis and discussion; G. Bai and G. Liu performed the EPR measurements and analysis; J. Fu and M. Tang led the project. All authors contributed to the manuscript and were involved in the discussion.

Conflicts of interest

There are no conflicts of interest to declare.

Acknowledgements

This work was financially supported by the National Natural Science Foundation of China (grants 22090043), Natural Science Foundation of Zhejiang Province (Grant no. LQ21E020006), and the Fundamental Research Funds for the Provincial Universities of Zhejiang (Grant no. 2021YW46). The authors kindly thank Dr Kuo Li for his insightful discussions as well as help from Shijing Zhao, Wenfeng Peng, Wenbo Cheng, Jingbo Nan and Mingxing Chen for PL and PLE data acquisition.

References

1 T. Hu, L. Ning, Y. Gao, J. Qiao, E. Song, Z. Chen, Y. Zhou, J. Wang, M. S. Molokeev, X. Ke, Z. Xia and Q. Zhang, Glass Crystallization Making Red Phosphor for High-Power Warm White Lighting, *Light: Sci. Appl.*, 2021, **10**(1), 56, DOI: 10.1038/s41377-021-00498-6.

2 H. Zhu, X. Huang, Y. Li, Y. She, J. Wang, W.-Y. Wong, M. Liu, W. Li, Z. Zhou and M. Xia, Novel Ultra-High-Temperature Zero-Thermal Quenching Plant-Protecting Type Blue-Green Dual-Emission $KAl_{11}O_{17}$:Eu^{2+},Mn^{2+} Phosphors for Urban Ecological Lighting, *J. Mater. Chem. C*, 2022, **10**(9), 3461–3471, DOI: 10.1039/D1TC04890B.

3 P. Pust, V. Weiler, C. Hecht, A. Tücks, A. S. Wochnik, A.-K. Henß, D. Wiechert, C. Scheu, P. J. Schmidt and W. Schnick, Narrow-Band Red-Emitting Sr[$LiAl_3N_4$]:Eu^{2+} as a next-Generation LED-Phosphor Material, *Nat. Mater.*, 2014, **13**(9), 891–896, DOI: 10.1038/nmat4012.

4 Z. Jia, C. Yuan, Y. Liu, X.-J. Wang, P. Sun, L. Wang, H. Jiang and J. Jiang, Strategies to Approach High Performance in Cr^{3+}-Doped Phosphors for High-Power NIR-LED Light Sources, *Light: Sci. Appl.*, 2020, **9**(1), 86, DOI: 10.1038/s41377-020-0326-8.

5 G. J. Hoerder, M. Seibald, D. Baumann, T. Schröder, S. Peschke, P. C. Schmid, T. Tyborski, P. Pust, I. Stoll, M. Bergler, C. Patzig, S. Reißaus, M. Krause, L. Berthold, T. Höche, D. Johrendt and H. Huppertz, Sr[$Li_2Al_2O_2N_2$]:Eu^{2+}—A High Performance Red Phosphor to Brighten the Future, *Nat. Commun.*, 2019, **10**(1), 1824, DOI: 10.1038/s41467-019-09632-w.

6 Q. Yao, P. Hu, P. Sun, M. Liu, R. Dong, K. Chao, Y. Liu, J. Jiang and H. Jiang, YAG:Ce^{3+} Transparent Ceramic Phosphors Brighten the Next-Generation Laser-Driven Lighting, *Adv. Mater.*, 2020, **32**(19), 1907888, DOI: 10.1002/adma.201907888.

7 S. Yang, B. Jiang, J. Wu, C. Duan, Y. Shan and Q. Zhao, $LaMoBO_6$:Tb^{3+},Eu^{3+}/Sm^{3+},Bi^{3+} Yellow Phosphors with Exceptionally High Quantum Yields That Can Be Excited by Blue Light, *J. Mater. Chem. C*, 2021, **9**(22), 7065–7073, DOI: 10.1039/D1TC00254F.

8 X. Zhang, Y.-T. Tsai, S.-M. Wu, Y.-C. Lin, J.-F. Lee, H.-S. Sheu, B.-M. Cheng and R.-S. Liu, Facile Atmospheric Pressure Synthesis of High Thermal Stability and Narrow-Band Red-Emitting $SrLiAl_3N_4$:Eu^{2+} Phosphor for High Color Rendering Index White Light-Emitting Diodes, *ACS Appl. Mater. Inter.*, 2016, **8**(30), 19612–19617, DOI: 10.1021/acsami.6b05485.

9 J. Fu, S. Zhang, R. Pang, Y. Jia, W. Sun, H. Li, L. Jiang and C. Li, Material and Ingenious Synthesis Strategy for Short-Wavelength Infrared Light-Emitting Device, *Inorg. Chem.*, 2016, **55**(21), 11258–11263, DOI: 10.1021/acs.inorgchem.6b01849.

10 J. Fu, S. Zhang, T. Ma, Y. Jia, R. Pang, L. Jiang, D. Li, H. Li, W. Sun and C. Li, A Convenient and Efficient Synthesis Method to Improve the Emission Intensity of Rare Earth Ion Doped Phosphors: The Synthesis and Luminescent Properties of Novel SrO:Ce^{3+} Phosphor, *RSC Adv.*, 2015, **5**(114), 93951–93956, DOI: 10.1039/C5RA15089B.

11 J. Fu, R. Pang, L. Jiang, Y. Jia, W. Sun, S. Zhang and C. Li, A Novel Dichromic Self-Referencing Optical Probe SrO:-Bi^{3+},Eu^{3+} for Temperature Spatially and Temporally Imaging, *Dalton Trans.*, 2016, **45**(34), 13317–13323, DOI: 10.1039/C6DT01552B.

12 X. Wang, Z. Qiu, Y. Liang, Z. Song, S. Li, J. Zhang and S. Lian, Achieving Dynamic Multicolor Luminescence in

ZnS:KBr,Mn^{2+} Phosphor for Anti-Counterfeiting, *Chem. Eng. J.*, 2022, **429**, 132537, DOI: 10.1016/j.cej.2021.132537.

13 Y. Gao, R. Li, W. Zheng, X. Shang, J. Wei, M. Zhang, J. Xu, W. You, Z. Chen and X. Chen, Broadband NIR Photostimulated Luminescence Nanoprobes Based on CaS:Eu^{2+},Sm^{3+} Nanocrystals, *Chem. Sci.*, 2019, **10**(21), 5452–5460, DOI: 10.1039/C9SC01321K.

14 S. Shim, W. B. Park, M. Kim, J. Lee, S. P. Singh and K.-S. Sohn, Cyan-Light-Emitting Chalcogenometallate Phosphor, $KGaS_2$:Eu^{2+}, for Phosphor-Converted White Light-Emitting Diodes, *Inorg. Chem.*, 2021, **60**(8), 6047–6056, DOI: 10.1021/acs.inorgchem.1c00509.

15 K. Ashwini, C. Pandurangappa, K. Avinash, S. Srinivasan and E. Stefanakos, Synthesis, Characterization and Photoluminescence Studies of Samarium Doped Zinc Sulfide Nanophosphors, *J. Lumin.*, 2020, **221**, 117097, DOI: 10.1016/j.jlumin.2020.117097.

16 A. M. Pires and M. R. Davolos, Luminescence of Europium(III) and Manganese(II) in Barium and Zinc Orthosilicate, *Chem. Mater.*, 2001, **13**(1), 21–27, DOI: 10.1021/cm000063g.

17 M. Zhao, H. Liao, M. S. Molokeev, Y. Zhou, Q. Zhang, Q. Liu and Z. Xia, Emerging Ultra-Narrow-Band Cyan-Emitting Phosphor for White LEDs with Enhanced Color Rendition, *Light: Sci. Appl.*, 2019, **8**, 38, DOI: 10.1038/s41377-019-0148-8.

18 J. J. Joos, D. Van der Heggen, L. I. D. J. Martin, L. Amidani, P. F. Smet, Z. Barandiarán and L. Seijo, Broadband Infrared LEDs Based on Europium-to-Terbium Charge Transfer Luminescence, *Nat. Commun.*, 2020, **11**(1), 3647, DOI: 10.1038/s41467-020-17469-x.

19 M.-H. Fang, J.-C. Lin, W.-T. Huang, N. Majewska, J. Barzowska, S. Mahlik, W. K. Pang, J.-F. Lee, H.-S. Sheu and R.-S. Liu, Linking Macro- and Micro-Structural Analysis with Luminescence Control in Oxynitride Phosphors for Light-Emitting Diodes, *Chem. Mater.*, 2021, **33**(19), 7897–7904, DOI: 10.1021/acs.chemmater.1c02990.

20 Z. Xia, C. Ma, M. S. Molokeev, Q. Liu, K. Rickert and K. R. Poeppelmeier, Chemical Unit Cosubstitution and Tuning of Photoluminescence in the $Ca_2(Al_{1-x}Mg_x)(Al_{1-x}Si_{1+x})O_7$:$Eu^{2+}$ Phosphor, *J. Am. Chem. Soc.*, 2015, **137**(39), 12494–12497, DOI: 10.1021/jacs.5b08315.

21 J. Qiao, G. Zhou, Y. Zhou, Q. Zhang and Z. Xia, Divalent Europium-Doped near-Infrared-Emitting Phosphor for Light-Emitting Diodes, *Nat. Commun.*, 2019, **10**(1), 5267, DOI: 10.1038/s41467-019-13293-0.

22 D. Zhang, W. Xiao, C. Liu, X. Liu, J. Ren, B. Xu and J. Qiu, Highly Efficient Phosphor-Glass Composites by Pressureless Sintering, *Nat. Commun.*, 2020, **11**(1), 2805, DOI: 10.1038/s41467-020-16649-z.

23 F. Ruegenberg, A. García-Fuente, M. Seibald, D. Baumann, S. Peschke, W. Urland, A. Meijerink, H. Huppertz and M. Suta, Chasing Down the Eu^{2+} Ions: The Delicate Structure–Property Relationships in the Ultra-Narrow Band Phosphor $K_{1.6}Na_{2.1}Li_{0.3}[Li_3SiO_4]4$:$Eu^{2+}$, *Adv. Opt. Mater.*, 2021, **9**(24), 2101643, DOI: 10.1002/adom.202101643.

24 C. Cheng, L. Ning, X. Ke, M. S. Molokeev, Z. Wang, G. Zhou, Y. Chuang and Z. Xia, Designing High-Performance LED Phosphors by Controlling the Phase Stability via a Heterovalent Substitution Strategy, *Adv. Opt. Mater.*, 2020, **8**(2), 1901608, DOI: 10.1002/adom.201901608.

25 Z. Mei, Q. Ni, M. Li, J. Li, J. Huo, W. Liu and Q. Wang, Extension of Spectral Shift Controls from Equivalent Substitution to an Energy Migration Model Based on Eu^{2+}/Tb^{3+}-Activated $Ba_{4-x}Sr_xGd_{3-x}Lu_xNa_3(PO_4)_6F_2$ Phosphors, *Inorg. Chem.*, 2021, **60**(21), 16507–16517, DOI: 10.1021/acs.inorgchem.1c02340.

26 J. J. Joos, P. F. Smet, L. Seijo and Z. Barandiarán, Insights into the Complexity of the Excited States of Eu-Doped Luminescent Materials, *Inorg. Chem. Front.*, 2020, **7**(4), 871–888, DOI: 10.1039/C9QI01455A.

27 S. Mahlik, T. Lesniewski, M. Grinberg, D. Kulesza and E. Zych, Spectroscopic Properties of High-Temperature Sintered SrS:0.05%Ce^{3+} under High Hydrostatic Pressure, *Phys. Chem. Chem. Phys.*, 2018, **20**(15), 10266–10274, DOI: 10.1039/C7CP08353J.

28 J. J. Joos, L. Seijo and Z. Barandiarán, Direct Evidence of Intervalence Charge-Transfer States of Eu-Doped Luminescent Materials, *J. Phys. Chem. Lett.*, 2019, **10**(7), 1581–1586, DOI: 10.1021/acs.jpclett.9b00342.

29 J. Tian and W. Zhuang, Thermal Stability of Nitride Phosphors for Light-Emitting Diodes, *Inorg. Chem. Front.*, 2021, **8**(22), 4933–4954, DOI: 10.1039/D1QI00993A.

30 H. Daicho, T. Iwasaki, K. Enomoto, Y. Sasaki, Y. Maeno, Y. Shinomiya, S. Aoyagi, E. Nishibori, M. Sakata, H. Sawa, S. Matsuishi and H. Hosono, A Novel Phosphor for Glareless White Light-Emitting Diodes, *Nat. Commun.*, 2012, **3**(1), 1132, DOI: 10.1038/ncomms2138.

31 Z. Xia, C. Ma, M. S. Molokeev, Q. Liu, K. Rickert and K. R. Poeppelmeier, Chemical Unit Cosubstitution and Tuning of Photoluminescence in the $Ca_2(Al_{1-x}Mg_x)(Al_{1-x}Si_{1+x})O7$:$Eu^{2+}$ Phosphor, *J. Am. Chem. Soc.*, 2015, **137**(39), 12494–12497, DOI: 10.1021/jacs.5b08315.

32 Y. Sato, H. Kato, M. Kobayashi, T. Masaki, D.-H. Yoon and M. Kakihana, Tailoring of Deep-Red Luminescence in Ca_2SiO_4:Eu^{2+}, *Angew. Chem., Int. Ed.*, 2014, **53**(30), 7756–7759, DOI: 10.1002/anie.201402520.

33 A. R. Kadam, G. C. Mishra, A. D. Deshmukh and S. J. Dhoble, Enhancement of Blue Emission in Ce^{3+}, Eu^{2+} Activated $BaSiF_6$ Downconversion Phosphor by Energy Transfer Mechanism: A Photochromic Phosphor, *J. Lumin.*, 2021, **229**, 117676, DOI: 10.1016/j.jlumin.2020.117676.

34 Y. Jia, R. Pang, H. Li, W. Sun, J. Fu, L. Jiang, S. Zhang, Q. Su, C. Li and R.-S. Liu, Single-Phased White-Light-Emitting $Ca_4(PO_4)_2O$:Ce^{3+},Eu^{2+} Phosphors Based on Energy Transfer, *Dalton Trans.*, 2015, **44**(25), 11399–11407, DOI: 10.1039/C5DT01018G.

35 D. O. A. dos Santos, L. Giordano, M. A. S. G. Barbará, M. C. Portes, C. C. S. Pedroso, V. C. Teixeira, M. Lastusaari and L. C. V. Rodrigues, Abnormal Co-Doping Effect on the Red Persistent Luminescence SrS:Eu^{2+},RE^{3+} Materials, *Dalton Trans.*, 2020, **49**(45), 16386–16393, DOI: 10.1039/D0DT01315C.

36 S. K. Gupta, M. K. Bhide, R. M. Kadam, V. Natarajan and S. V. Godbole, Nanorods of White Light Emitting Sr_2SiO_4:Eu^{2+}: Microemulsion-Based Synthesis, EPR, Photoluminescence, and Thermoluminescence Studies, *J. Exp. Nanosci.*, 2015, **10**(8), 610–621, DOI: 10.1080/17458080.2013.858833.

37 L. Havlák, V. Jarý, J. Bárta, M. Buryi, M. Rejman, V. Laguta and M. Nikl, Tunable Eu^{2+} Emission in $K_xNa_{1-x}LuS_2$ Phosphors for White LED Application, *Mater. Design.*, 2016, **106**, 363–370, DOI: **10.1016/j.matdes.2016.05.123**.

38 Y. Tan and C. Shi, $Ce^{3+} \rightarrow Eu^{2+}$ Energy Transfer in $BaLiF_3$ Phosphor, *J. Phys. Chem. Solids*, 1999, **60**(11), 1805–1810, DOI: **10.1016/S0022-3697(99)00200-0**.

39 C.-K. Chang and T.-M. Chen, $Sr_3B_2O_6:Ce^{3+},Eu^{2+}$: A Potential Single-Phased White-Emitting Borate Phosphor for Ultraviolet Light-Emitting Diodes, *Appl. Phys. Lett.*, 2007, **91**(8), 081902, DOI: **10.1063/1.2772195**.

40 X. Zhang, D. Zhang, B. Zheng, Z. Zheng, Y. Song, K. Zheng, Y. Sheng, Z. Shi and H. Zou, Luminescence and Energy Transfer of Color-Tunable $Y_2Mg_2Al_2Si_2O_{12}:Eu^{2+},Ce^{3+}$ Phosphors, *Inorg. Chem.*, 2021, **60**(8), 5908–5916, DOI: **10.1021/acs.inorgchem.1c00317**.

41 D. Jia and X. Wang, Alkali Earth Sulfide Phosphors Doped with Eu^{2+} and Ce^{3+} for LEDs, *Opt. Mater.*, 2007, **30**(3), 375–379, DOI: **10.1016/j.optmat.2006.11.061**.

42 D. Jia, Enhancement of Long-Persistence by Ce Co-Doping in $CaS:Eu^{2+},Tm^{3+}$ Red Phosphor, *J. Electrochem. Soc.*, 2006, **153**, 198–201, DOI: **10.1149/1.2337087**.